Excited-State Dynamics of Chlorine Dioxide in the Condensed Phase from Resonance Raman Intensities

Anthony P. Esposito, Catherine E. Foster, Robert A. Beckman, and Philip J. Reid*

Department of Chemistry, Box 351700, University of Washington, Seattle, Washington 98195

Received: November 5, 1996; In Final Form: May 6, 1997[⊗]

Resonance Raman spectra of chlorine dioxide (OClO) dissolved in cyclohexane obtained with excitation throughout the $^2B_1-{}^2A_2$ electronic transition are presented. Resonance Raman intensity corresponding to all vibrational degrees of freedom (the symmetric stretch, bend, and asymmetric stretch) is observed, demonstrating that excited-state structural evolution along all three coordinates occurs upon photoexcitation. The electronic absorption and absolute resonance Raman cross sections are reproduced employing the time-dependent formalism for Raman scattering using an anharmonic description of the $^2A_2$, excited-state potential-energy surface. Analysis of the resonance Raman cross-sections demonstrates that both homogeneous and inhomogeneous broadening mechanisms are operative in cyclohexane. Comparison of the experimentally determined, gas-phase $^2A_2$ surface to that in solution defined by the analysis presented here shows that although displacements along the symmetric stretch and bend are similar in both phases, evolution along the asymmetric stretch is dramatically altered in solution. Specifically, employing the gas-phase potential along this coordinate, the predicted intensity of the overtone transition is an order of magnitude larger than that observed. The analysis presented here demonstrates that the asymmetric stretch overtone intensity is consistent with a reduction in excited-state frequency along this coordinate from 1100 to 750 ± 100 cm^{-1}. This comparison suggests that differences in evolution along the asymmetric stretch may be responsible for the phase-dependent reactivity of OClO. In particular, the absence of substantial evolution along the asymmetric stretch in solution results in the ground-state symmetry of OClO being maintained in the $^2A_2$ excited state. The role of symmetry in defining the reaction coordinate and the nature of the solvent interaction responsible for modulation of the excited-state potential energy surface are discussed.

Introduction

Understanding phase- and environment-dependent chemical reactivity is a central issue in environmental chemistry.[1,2] This area of environmental chemistry is closely related to current research in chemical physics involved in elucidating the role of solvent in condensed-phase chemical processes.[3] Progress in both areas is dependent on defining the microscopic details of solvent−solute interactions which influence reaction rates and product yields. The importance of solvent effects in environmental processes is elegantly illustrated by the photochemistry of chlorine dioxide (OClO).[4]

Scheme 1 outlines the photochemical reactivity of OClO. Photoexcitation results either in bond cleavage to form ClO and atomic oxygen or in the formation of molecular oxygen and atomic chlorine.[4−36] It is the latter photochemical pathway that is responsible for the environmental impact of OClO. In atmospheric chemistry, photodecomposition of OClO may represent an important source of atomic chlorine, which can participate in stratospheric ozone depletion.[4,10,37−39] In aquifer chemistry, OClO has been utilized in water purification and paper manufacturing, but recent studies suggest that this compound may actually serve as an aquifer contaminant since atomic chlorine is involved in the formation of toxic and mutagenic polychlorinated species.[40−44]

The intriguing aspect of OClO chemistry is that the quantum yield for Cl production is phase dependent. Numerous investigations on the gas-phase reactivity of OClO have established that in this phase, photoexcitation leads predominately to the formation of ClO and O.[8,9,16,18−20,22,25,26,45−47] The minor

SCHEME 1

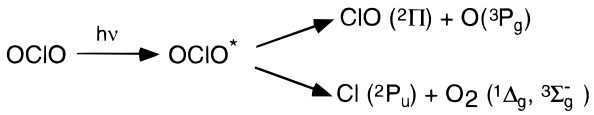

reaction pathway corresponding to Cl + O_2 formation is believed to proceed via photoisomerization of OClO to ClOO with subsequent decomposition of this species resulting in product formation.[4,12,28,29,33−36] The gas-phase photochemical quantum yield for this process remains the subject of debate with values ranging from 0.15 to ∼0.[10,15−17,20,21] In contrast, matrix isolation studies have demonstrated that photoexcitation of OClO results quantitatively in the formation of ClOO.[5,6,28,30−35,48] The importance of geminate recombination in matrix photochemistry remains unclear; however, the quantum yield for ClOO formation in matrixes of both weakly (Ar) and strongly (H_2SO_4, H_2O) associating molecules is the same suggesting that solvent "caging" effects are minimal.[31−33] Furthermore, recent experiments on OClO adsorbed to polycrystalline Pt have demonstrated that the O_2 and Cl photoproducts are released from the surface with hyperthermal energies, suggesting that these products are produced directly rather than by the ground-state decomposition of ClOO.[30]

Although the gas-phase and matrix chemistry of OClO has been extensively investigated, the solution-phase reaction dynamics of OClO have only recently been explored.[11−14,49] Pioneering research by Simon and co-workers has established that the quantum yield for ClOO formation in polar solution is 0.1−0.2.[11,12] Furthermore, this work established the direct production of ClOO from the photolysis of OClO in water and placed a limit of ∼1 ps on the appearance time for ground-

* To whom correspondence should be addressed.

[⊗] Abstract published in *Advance ACS Abstracts,* July 1, 1997.

S1089-5639(96)03703-6 CCC: $14.00

state ClOO. However, convolution of the photoproduct appearance and vibrational relaxation kinetics prohibited an absolute determination of the photoproduct formation rate.[11]

The phenomenology of OClO photochemistry has been established; however, the mechanistic details responsible for the phase-dependent reactivity remain unknown. In particular, issues such as the nuclear dimensionality of the initial, excited-state evolution, the excited-state decay rate, the kinetics of photoproduct formation, and the influence of solvent on these processes remain unanswered. In this paper, we present the results of our initial investigations on the condensed-phase reaction dynamics of OClO. Specifically, resonance Raman intensity analysis is employed to determine the early-time, excited-state reaction dynamics. This work represents our initial step in systematically defining how solvents influence the chemistry of halooxides in condensed environments. The information obtained from these investigations will assist in developing an understanding of halooxide chemistry in both homogeneous and heterogeneous settings.

Analysis of the resonance Raman intensities of OClO dissolved in cyclohexane demonstrates that relative to the gas phase, the nuclear evolution which occurs on the optically prepared, excited-state potential energy surface is dramatically altered in solution. Specifically, the large structural change along the asymmetric stretch coordinate present in the gas-phase occurs only to a limited extent in solution, resulting in the preservation of the ground-state symmetry of OClO in the $^2A_2$ excited state. The difference in structural evolution combined with previous results on OClO photochemistry indicates that in cyclohexane, the conservation of ground-state symmetry is responsible for the production of Cl and O_2 by a symmetric dissociation mechanism as opposed to product formation via the lower symmetry, ClOO intermediate. In addition, the results presented here imply that the dynamics which occur on the predissociative, $^2A_2$ surface are important in defining the phase-dependent reactivity of OClO.

Experimental Section

Materials. Chlorine dioxide (OClO) was synthesized by published methods.[50] Briefly, 13.6 g of potassium chlorate (99+% reagent grade, Aldrich) and 11.1 g of oxalic acid dihydrate (reagent grade, J. T. Baker) were dissolved in 60 mL of 2.3 M sulfuric acid (98% reagent grade, J. T. Baker). The solution was continuously stirred and slowly heated in a water bath until the evolution of green, gaseous OClO was observed. The OClO gas was passed through a drying tube containing phosphorus pentoxide (reagent grade, J. T. Baker) and bubbled through 250 mL of neat cyclohexane (spectrophotometric grade, J. T. Baker) cooled to ~6 °C. This procedure resulted in a OClO concentration of ~100 mM with concentration and prep purity determined by static vis−UV absorption. Gaseous OClO is known to readily explode at pressures greater than 30 Torr; therefore, great care must be taken during preparation. Neat OClO was isolated for use in determination of the absorption cross section in cyclohexane (see below). The preparation of OClO was performed similar to that described above except that after drying, OClO was trapped in a 10 mL flask cooled to −38 °C using a dry ice/xylenes slush bath. This arrangement resulted in the condensation of OClO (boiling point: 11 °C) while coproduced CO_2 passed through the collection flask.[51] Calibrated capillary pipets were precooled in liquid nitrogen and used to transfer the liquid OClO into volumetric flasks for dilution and determination of the cross section. Extreme care must be taken in the transfer of liquid OClO, where vaporization typically results in explosion.

Resonance Raman Spectra. Excitation at 532, 435.7, 368.9, 355, 319.9, and 282.4 nm was provided by the direct and hydrogen-shifted, second and third harmonic output of a Nd:YAG laser (Spectra-Physics GCR-170) operating at 30 Hz. Power dependence of the OClO scattering was monitored at 368.9 nm by measuring the scattering intensity of the symmetric stretch versus incident power. A linear increase with intensity up to 10 μJ/pulse was observed, at which point the onset of ground-state depletion was observed. Pulse energies were kept to <10 μJ at 368.9 nm and adjusted at other wavelengths by scaling this pulse energy by the absorption cross section to maintain a homogeneous extent of photoalteration at all excitation points. The incident light was focused onto either a thin-film, wire-guided jet of the OClO solution (368.9, 355, 319.9, and 282.4 nm) or glass capillary containing the OClO solution (532, 435.7, 368.9, and 355 nm) using a 100 mm focal length, UV-quality spherical lens. Sample flow rates were sufficient to replace the illuminated sample volume between excitation pulses. The scattered light was collected and delivered to a 0.5 m spectrograph (Acton) using refractive, UV-quality optics. A polarization scrambler was placed before the entrance of the spectrograph to minimize the polarization dependence of the spectrograph throughput. The scattered light was dispersed using either a 1200 g/mm classically ruled ($\lambda_b = 500$ nm) or a 2400 g/mm holographic grating. Typical entrance slit widths of 75 μm resulted in a spectral band-pass of 8 cm^{-1}. The scattered light was detected with a Princeton Instruments, liquid nitrogen cooled, back-thinned, 1100 × 330 pixel CCD detector.

Depolarization Ratios. The resonance Raman depolarization ratio of the OClO symmetric stretch fundamental transition was measured at all excitation wavelengths. The depolarization ratio is defined as the intensity of scattered light with polarization perpendicular to that of the incident radiation divided by the intensity of scattered light with parallel polarization.[52] The polarization of the incident light was defined by passing the excitation light through a stack of five, air-spaced quartz microscope slides oriented at the Brewster's angle, resulting in a polarization contrast ratio >1000:1. The polarization of the scattered light was analyzed using a large aperture (1.5 cm) Glan-Taylor calcite polarizer placed before the polarization scrambler. Measurement of the depolarization ratio of the 802 cm^{-1} line of cyclohexane resulted in a value of 0.09 ± 0.01, in agreement with previously published results.[53]

Intensity Corrections. All resonance Raman spectra were corrected for wavelength-dependent sensitivity using standard D_2 emission (Hellma) or quartz−tungsten−halogen (Oriel) lamps. The spectra were corrected for self-absorption using the following analytic function:[54,55]

$$I_0 = \frac{I(\epsilon\chi + \epsilon_\lambda)}{1 - \exp(-2.3bc(\epsilon\chi + \epsilon_l))} \quad (1)$$

where I_0 is the corrected intensity; I is the uncorrected intensity; ϵ and ϵ_l are the extinction coefficients at the scattered and laser frequencies, respectively; b is the path length (the diameter of the capillary or thickness of the jet); c is the concentration; and χ is a geometric factor that accounts for the difference in path lengths between the incident and scattered light in the "135° backscattering" arrangement and is given by

$$\chi = \sin[\cos^{-1}(R\cos\theta)] \quad (2)$$

where R is the ratio of the index of refraction of air relative to cyclohexane and θ is the angle between the incident light and the sample surface. Measurement of the actual geometry employed in the experiments resulted in a typcial value for χ

TABLE 1: Measured Raman Cross Sections for Chlorine Dioxide in Cyclohexane

excitation energy ($\times 10^{-3}$ cm^{-1})	ν_1 ($\times 10^{10}$ Å^2)[a]	$2\nu_1$ ($\times 10^{10}$ Å^2)	ν_2 ($\times 10^{10}$ Å^2)	$2\nu_3$ ($\times 10^{10}$ Å^2)	$\rho(\nu_1)$[b]
18.8 (532.0 nm)	0.05 ± 0.07[c]				0.11 ± 0.01
23.0 (435.7 nm)	1.62 ± 0.22	1.28 ± 0.19			0.20 ± 0.02
27.1 (368.9 nm)	6.90 ± 1.40	3.75 ± 0.81	0.97 ± 0.24	0.37 ± 0.06	0.25 ± 0.04
28.2 (355.0 nm)	7.00 ± 1.40	8.78 ± 1.50		0.46 ± 0.08	0.22 ± 0.03
31.3 (319.9 nm)	9.54 ± 1.20	4.62 ± 1.40	0.20 ± 0.07		0.19 ± 0.02
35.4 (282.4 nm)	2.40 ± 0.28	0.80 ± 0.31			0.18 ± 0.02

[a] Absolute intensities were determined by comparison to the 802 cm^{-1} line of cyclohexane for which absolute Raman intensities are known.[53,96] [b] The Raman depolarization ratio for the symmetric stretch. This ratio is the Raman intensity observed perpendicular to the polarization axis of the incident light divided by the Raman intensity observed parallel to this axis. [c] Errors represent 1 standard deviation from the mean.

of 0.89 ± 0.04. Finally, the correction for chromatic aberration was performed by comparison of solvent line intensities between spectra of neat cyclohexane and spectra with OClO present with this correction resulting in a ≤3% change in intensities. The absolute resonance Raman intensity of the symmetric stretch fundamental and overtone transition of OClO was determined at each excitation wavelength by comparison to the 802 cm^{-1} line of cyclohexane using the following equation:[54]

$$\frac{\sigma_{\mathrm{OClO}}}{\sigma_{\mathrm{CXN}}} = \frac{(I_{\mathrm{OClO}})(c_{\mathrm{CXN}})[(1+2\rho)/(1+\rho)]_{\mathrm{OClO}}}{(I_{\mathrm{CXN}})(c_{\mathrm{OClO}})[(1+2\rho)/(1+\rho)]_{\mathrm{CXN}}} \qquad (3)$$

where σ is the Raman cross section, I is the scattered intensity, c is the concentration, and ρ is the Raman depolarization ratio. Observed intensities were determined by simple integration of peak areas and by a nonlinear, least-squares fit of the spectra to a sum of Gaussian peaks convolved with a Lorentzian instrument response and linear background. Intensities determined using either approach produced equivalent resonance Raman cross sections to within experimental error. Intensities of transitions other than the fundamental and overtone of the symmetric stretch were determined by comparison to the symmetric stretch fundamental. The results of this analysis are presented in Table 1.

Data Analysis

The absorption and Raman excitation spectra were modeled under the assumption that the observed scattering is dominated by the $^2A_2$ excited state and that contributions from other states are negligible. Deviation of the Raman depolarization ratios from 0.33 (Table 1), the value when only a single electronic state contributes to the observed scattering, demonstrates that this assumption is only approximate for OClO. The depolarization ratios observed with excitation at 355 ($\rho = 0.22 \pm 0.03$) and 368.9 nm ($\rho = 0.25 \pm 0.04$) were closest to 0.33 and indicate that the single-state approximation is most valid at these wavelengths. Therefore, refinement of the calculation was performed with reference to the Raman cross sections measured at these excitation points. We have recently completed an analysis of the wavelength-dependent Raman depolarization ratios for the symmetric stretch fundamental transition of OClO dissolved in cyclohexane with a detailed description of this work to appear shortly.[56] To briefly summarize the results of this study, the observed wavelength dependence of the depolarization ratios could be reproduced if the optically weak, $^2A_1$, potential energy surface also contributes to the observed scattering. However, the smaller transition moment and larger homogeneous line width of this surface results in the $^2A_1$ state making only a modest contribution to the observed intensities. Specifically, the main adjustment in the parameters reported here is a 10% reduction in the electronic transition length with the description of the $^2A_2$ potential energy surface remaining unchanged. Therefore, the single state approximation employed in this analysis is judged to be appropriate.

The Raman excitation profiles and electronic absorption spectrum were modeled using the time-dependent formalism of Lee and Heller.[57−61] In this approach, the Raman cross section is given by the following:

$$\sigma_{\mathrm{R}}(E_{\mathrm{l}}) = \frac{8\pi E_{\mathrm{s}}{}^3 E_{\mathrm{l}} e^4 M_{\mathrm{eg}}^4}{9h^6c^4} \int_{-\infty}^{\infty} \partial E_0\, H(E_0) \left| \int_0^{\infty} \langle f|i(t)\rangle \times \exp[i(E_{\mathrm{l}} + E_{\mathrm{i}})t/h] D(t)\, \mathrm{d}t \right|^2 \qquad (4)$$

where E_{s} and E_{l} are the frequencies of the scattered and incident light, respectively; E_{i} is the energy of the initial vibrational state, M_{eg} is the electronic transition moment, and $\langle f|i(t)\rangle$ represents the time-dependent overlap of the final state in the scattering process with the initial vibrational state propagating under the influence of the excited-state Hamiltonian. The lowest frequency vibrational mode of OClO is at 450 cm^{-1}; therefore, the initial vibrational state for all vibrational degrees of freedom was taken to be the ground vibrational level (the "0 K" approximation). The damping function, $D(t)$, is composite of both radiative and nonradiative vibronic dephasing processes corresponding to both population decay (T_1) and pure-dephasing (T_2*). In general, $D(t)$ is expected to be a single-exponential decay with a time constant corresponding to the optical T_2; however, Gaussian and more complex forms have also been employed.[60,62,63] The analysis presented here was performed with both Gaussian and Lorentzian line shapes; however, the calculations employing a Gaussian line width typically resulted in better agreement with the data (see below). Although the origin of a Gaussian functional form for the homogeneous line width is not explicitly treated in this study, the Brownian oscillator model for solvent-induced dephasing is capable of reproducing this line width when solvent fluctuations are slower than the time scale for optical dephasing.[63] Finally, $H(E_0)$ is a Gaussian function which is included to model inhomogeneous broadening effects involving site differences which result in shifting of the energy gap between the ground and excited state (E_0). The inhomogeneous line width parameters reported here correspond to the standard deviation of the Gaussian distribution of solvent sites. The absorption cross section at the same level of approximation is

$$\sigma_{\mathrm{A}}(E_{\mathrm{l}}) = \frac{4\pi e^2 E_{\mathrm{l}} M_{\mathrm{eg}}{}^2}{6h^2cn} \int_{-\infty}^{\infty} \partial E_0\, H(E_0) \int_{-\infty}^{\infty} \langle i|i(t)\rangle \times \exp[i(E_{\mathrm{l}} + E_{\mathrm{i}})t/h] D(t)\, \mathrm{d}t \qquad (5)$$

where $\langle i|i(t)\rangle$ is the time-dependent overlap of the initial ground vibrational state with this same state propagating on the excited-state potential energy surface and n is the index of refraction. As is evident from the above equations, the Raman and absorption cross sections are dependent on the same excited-

state parameters; therefore, modeling of both Raman and absorption cross sections results in a self-consistent picture of the excited-state potential energy surface.

The "simple-harmonic" approximation, in which the potential energy surfaces are modeled as a quadratic function of the normal coordinates with each vibrational degree of freedom fully characterized by a single frequency (equal in the ground and excited state) and dimensionless displacement of the excited-state potential energy surface minimum relative to the ground state (Δ), is typically employed in the analysis of resonance Raman intensities.[60,61] However, this approximation is inadequate for OClO given the importance of anharmonicity in describing the potential energy surfaces (see below); therefore, the following excited-state potential energy surface in the ground-state dimensionless coordinate basis was employed:

$$V_e = \frac{1}{2}\frac{{\omega_{e1}}^2}{\omega_{g1}}(q_1 - \Delta_1)^2 + \frac{1}{2}\frac{{\omega_{e2}}^2}{\omega_{g2}}(q_2 - \Delta_2)^2 + \frac{1}{2}\frac{{\omega_{e3}}^2}{\omega_{g3}}(q_3)^2 + \frac{1}{6}\chi_{111}\left(\frac{\omega_{e1}}{\omega_{g1}}\right)^{3/2}(q_1 - \Delta_1)^3 + \frac{1}{2}\chi_{133}\left(\frac{\omega_{e1}}{\omega_{g1}}\right)^{1/2}\left(\frac{\omega_{e3}}{\omega_{g3}}\right)(q_1 - \Delta_1)(q_3)^2 + A\exp\left(-a^2{q_3}^2\frac{\omega_{e3}}{\omega_{g3}}\right) \quad (6)$$

where the subscripts 1, 2, and 3 refer to the symmetric stretch, bend, and asymmetric stretch, respectively. In addition, ω_e and ω_g denote the excited- and ground-state harmonic frequencies, respectively. In the above potential, the symmetric stretch coodinate is described by both harmonic and cubic anharmonic terms. The asymmetric stretch is modeled as harmonic with a Gaussian barrier as proposed by Richard and Vaida.[8] Given the limited displacement along the bend (see below), only the harmonic term along this coordinate is included such that this degree of freedom is separable from the stretch coordinates. Coupling between the symmetric and asymmetric stretch is incorporated with a cubic anharmonic term. Estimates for the magnitude of χ_{133} from analysis of the gas-phase absorption spectrum assuming harmonic potential energy surfaces suggest that it is of the same magnitude as χ_{111}.[8] Calculations were performed adjusting χ_{133} from 0 to $2\chi_{111}$ resulting in a 15% depression in the resonance Raman cross sections over this range. Since the effect of χ_{133} is small, this term was not included in the fits reported here in order to improve the efficiency of the calculation. In this limit, the three vibronic degrees of freedom are separable such that the multidimensional, time-dependent overlap was decomposed into products involving one-dimensional overlaps:

$$\langle i|i(t)\rangle = \prod_{k=1}^{3}\langle i_k|i_k(t)\rangle \quad (7)$$

$$\langle f|i(t)\rangle = \langle f_1|i_1(t)\rangle\prod_{k=2}^{3}\langle i_k|i_k(t)\rangle \quad (8)$$

where the subscript 1 denotes the Raman-active coordinate. A harmonic desciption of the ground-state surface along all three normal coordinates was employed. The time-dependent overlaps involving harmonic surfaces with frequency change were calculated using the method of Mukamel and co-workers.[64] Time-dependent overlaps for the anharmonic potentials were calculated using the approximate time-propagator method of Feit and Fleck.[65,66] In this approach, $|i(t)\rangle$ is given by

$$|i(t)\rangle = \exp(i(\Delta t)\nabla^2/4M)\exp(-i(\Delta t)V)\exp(i(\Delta t)\nabla^2/4M)|i(0)\rangle + \vartheta(\Delta t^3) \quad (9)$$

where ∇^2 is the Laplacian in position space, V is the excited-state potential, and Δt is the size of the propagation time step. The error in this approach scales as the cube of the time step; therefore, the step size was kept to a minimum (0.2 fs) with propagations employing 2500 time steps. For two-dimensional calculations performed when anharmonic coupling between the symmetric and asymmetric stretch coordinates is included in the description of the excited-state potential energy surface, a 600×600 grid was employed using 1000 steps of 0.5 fs/step to determine the overlap. In either case, the calculated intensities did not change with further increase in the number of time steps or a reduction in the step size. Finally, the Feit and Fleck propagator routine was checked by comparison to calculations involving displaced harmonic potentials as well as nondisplaced potentials with an unbound excited-state surface for which analytic solutions are known.[58,60]

Results

Electronic Absorption Spectra. The electronic absorption spectrum of OClO dissolved in cyclohexane measured in the region of the $^2B_1 - {}^2A_2$ transition is presented in Figure 1. To our knowledge, the absorption spectrum of OClO in this solvent has not been reported; therefore, this measurement was performed in order to complete the analysis presented below. The observed structure originates from progressions involving the symmetric stretch.[8,9,27] Figure 2 presents the comparison of the gas-phase spectrum of OClO to that observed in cyclohexane. Transitions involving excitation of both the symmetric stretch in combination with the bend or asymmetric stretch which are observed in the gas-phase spectrum are not seen in solution due to the increase in broadening in the condensed phase. This broadening prohibits analysis of the absorption spectrum alone in order to investigate the excited-state potential energy surface along the bend and asymmetric stretch coordinates. Although the absorption spectrum of OClO in cyclohexane is more diffuse than the gas-phase spectrum, it should be noted that the structured spectrum in cyclohexane stands in contrast to the relatively unstructured spectrum observed in water demonstrating that the observed broadening is solvent dependent (see below).[67] The maximum absorption cross section for OClO in cyclohexane is 0.042 Å^2, very close to the value determined for OClO in water and that determined from electron-energy-loss spectroscopy.[68,69]

Resonance Raman Intensity Analysis. The resonance Raman spectrum of OClO obtained with excitation at 368.9 nm is presented in Figure 3. The absolute Raman cross sections observed at all excitation wavelengths employed in this study are presented in Table 1. Transitions involving the symmetric stretch, bend, and asymmetric stretch are observed with the analysis of each discussed below.

Symmetric Stretch. The most prominent features of the spectra involve transitions corresponding to the symmetric stretch with both the fundamental (938 cm^{-1}) and overtone (1874 cm^{-1}) of this mode readily apparent. The large intensity of these transitions combined with the observed structure in the absorption spectrum demonstrates that evolution along this coordinate is a major component of the structural relaxation occurring on the optically prepared, excited-state potential energy surface. The vibrational frequencies observed here are in agreement with previously reported values.[8,33,34,70,71] Isotope splitting of the overtone band is evident, with the intensities

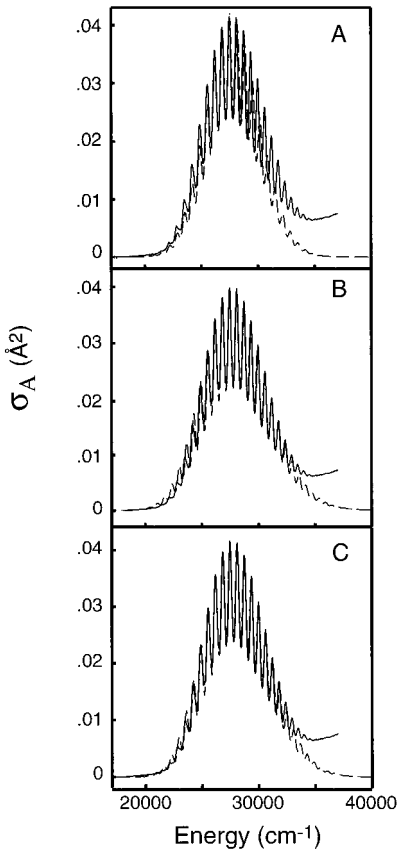

Figure 1. Experimental (solid) and calculated (dashed) electronic absorption spectra of chlorine dioxide (OClO) in cyclohexane. Calculated spectra are from analysis employing (A) Gaussian homogeneous broadening and a harmonic model of the excited-state potential energy surface, (B) Lorentzian homogeneous broadening and an anharmonic model of the excited-state potential energy surface, and (C) Gaussian homogeneous broadening and an anharmonic model of the excited-state potential energy surface. Time-dependent formalism and potentials used in the calculation are discussed in the text. Parameters used in the calculations incorporating an anharmonic description of the potential energy surface are presented in Table 2.

consistent with the natural abundance of ^{35}Cl and ^{37}Cl. In the analysis presented below, isotope splitting is not explicitly modeled and frequencies used in the calculation correspond to transitions involving the ^{35}Cl isotope.

Valence Bend. Limited intensity is observed in the fundamental of the bend at 450 cm^{-1} (Figure 3). The weak fundamental intensity of this mode is consistent with the limited excited-state displacement along this coordinate.[8,27] Previous electronic absorption analyses of OClO have qualitatively explained this small displacement as originating from the joint stretching and bending character of this mode with bond length and angle changes of opposite phase limiting the actual excited-state geometric distortion.[27] The overtone of the bend is also observed (~900 cm^{-1}), but the intensity of this transition was not determined since it is dominated by the nearby fundamental of the symmetric stretch.

Asymmetric Stretch. The ground-state symmetry of OClO is C_{2v}; therefore, fundamental intensity involving the asymmetric stretch is not predicted on resonance. However, differences in the curvature of the excited-state potential energy surface relative to that of the ground state can give rise to overtone intensity along this coordinate.[71] The expanded portion of Figure 3 presents the overtone region of the Raman spectrum. Intensity is observed at 2190 cm^{-1} and assigned to the overtone of the asymmetric stretch in agreement with the previous preresonance Raman work.[70]

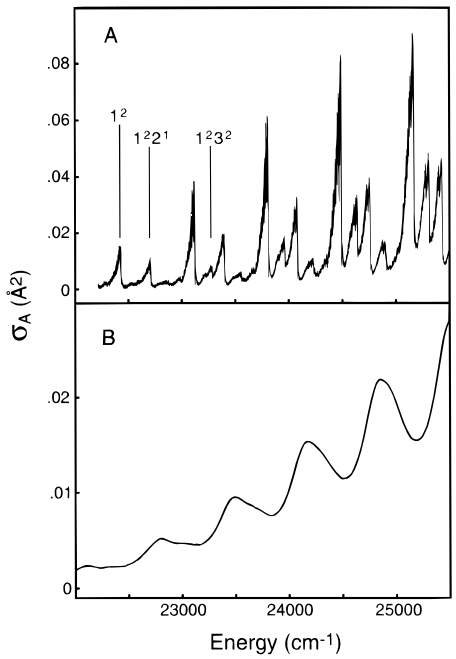

Figure 2. (A) Gas-phase absorption spectrum of OClO at 200 K reported by Vaida and co-workers.[8] A progression of transitions involving the symmetric stretch (1) in combination with the bend (2) and asymmetric stretch (3) is shown with the superscript defining the excited-state vibrational level to which the transition occurs. (B) Expanded view of the absorption spectrum of OClO in cyclohexane determined in this study.

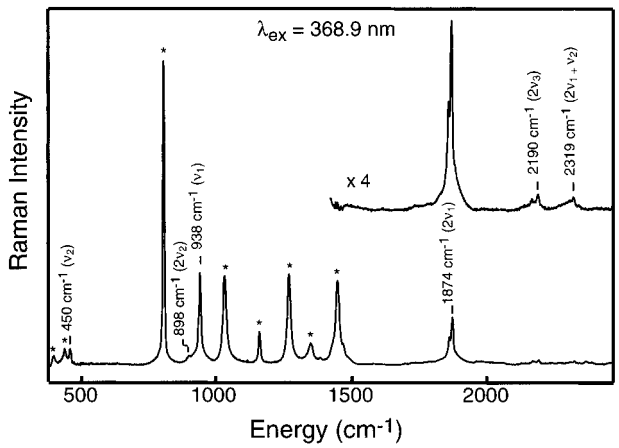

Figure 3. Resonance Raman spectrum of OClO in cyclohexane obtained with 368.9 nm excitation. Peaks marked with an asterisk are due to the cyclohexane solvent. Intensity assignable to all three coordinates (ν_1, symmetric stretch; ν_2, bend; ν_3, asymmetric stretch) is observed demonstrating that structural evolution occurs along all three coordinates upon photoexcitation. Expansion of the overtone region of the spectrum (with solvent subtracted) is presented demonstrating the presence of the asymmetric stretch overtone ($2\nu_3$).

Modeling of the $^2A_2$ Surface. Figure 1 presents the calculated electronic absorption spectrum from the time-dependent analysis presented above employing either Lorentzian or Gaussian homogeneous broadening. The excited-state potential energy surface parameters determined from this analysis are presented in Table 2. As noted above, initial attempts to model the data using harmonic potentials were unsuccessful in reproducing the frequencies of vibronic progressions observed in the electronic absorption spectrum demonstrating the importance of anharmonicity in describing the $^2A_2$ surface along the symmetric stretch coordinate (Figure 1A). Therefore, anharmonicity was included in the description of the $^2A_2$ state with the extent of anharmonicity determined by comparison to the

TABLE 2: $^2A_2$ Excited-State Potential Energy Surface Parameters for OClO in Cyclohexane

transition[b]	ω_g (cm^{-1})[c]	ω_e (cm^{-1})	Δ[d]	anharm[e] (cm^{-1})	σ_R(exp)[f] ($\times 10^{10}$ Å^2)	σ_R(calc) ($\times 10^{10}$ Å^2)
			Lorentzian[a]			
ν_1	938	675	6.2	−14	6.91	6.51
ν_2	450	284	0.3	0	0.97	0.80
ν_3	1100	750	0	0		
$2\nu_1$					3.75	2.9
$2\nu_3$					0.37	0.17
			Gaussian[g]			
ν_1	938	675	6.1	−14	6.90	6.90
ν_2	450	284	0.3	0	0.97	1.02
ν_3	1100	750	0	0		
$2\nu_1$					3.75	4.45
$2\nu_3$					0.37	0.29

[a] Calculation perfomed with a Lorentzian homogeneous line width. Best fit to the experimental cross sections resulted in $\Gamma = 90 \pm 15$ cm^{-1}, inhomogeneous standard deviation $= 140 \pm 20$ cm^{-1}, $E_{00} = 16\,750$ cm^{-1}, $M_{eg} = 0.35$ Å, $n = 1.42$. [b] Raman transition for which the calculation is performed. The symbols ν_1, ν_2, and ν_3 refer to the symmetric stretch, bend, and asymmetric stretch, respectively. The first three terms correspond to fundamental transitions, and the latter two terms refer to overtone transitions. [c] ω_g refers to the ground-state harmonic frequency, and ω_e is the excited-state harmonic frequency. [d] Values for the dimensionless displacement of the excited-state potential energy surface minimum relative to the ground state. [e] Anharmonicity prefactor for the cubic term in the series expansion of the potential energy surface. By comparison to the description of the Morse oscillator, this term is equal to $(w_e/2)^{1.5}/D_e^{0.5}$ in dimensionless units, where w_e is the excited-state harmonic frequency and D_e is the Morse dissociation energy given by $w_e^2/(4w_ex_e)$ where x_e is the anharmonicity parameter.[97] [f] Experimental Raman cross section corresponding to 368.9 nm excitation. [g] Calculation performed with a Gaussian homogeneous line width. Best fit to the experimental cross sections resulted in $\Gamma = 80 \pm 15$ cm^{-1}, inhomogeneous standard deviation $= 160 \pm 20$ cm^{-1}, $E_{00} = 17\,400$ cm^{-1}, $M_{eg} = 0.35$ Å, $n = 1.42$.

absorption spectrum. The absorption and Raman cross section data were first modeled utilizing an exponential form for the homogeneous line width (i.e., Lorentzian broadening); however, inspection of the experimental and calculated absorption spectra (Figure 1B) reveals that the intensity at the low-frequency edge of the absorption band is not well reproduced by this functional form. Use of Gaussian homogeneous broadening resulted in slightly better agreement between the calculated and observed absorption spectra (Figure 1C). In addition, the Raman cross sections obtained at the lower frequency excitation points were better reproduced. Therefore, the remaining presentation of the analysis is limited to calculations employing a Gaussian homogeneous line width. However, the differences between these two approaches are subtle, and the main conclusions presented below are unaffected by the choice of $D(t)$.

Figure 4 presents the calculated Raman excitation profile for the fundamental and overtone transitions of the symmetric stretch. If all broadening is incorporated as homogeneous, the predicted Raman cross sections are systematically lower than those observed. This indicates that the amount of homogeneous broadening used in the calculation is too large. Therefore, both homogeneous and inhomogeneous broadening were employed to simultaneously reproduce the Raman cross sections and the electronic absorption spectrum.[60] Since the electronic absorption is normalized with respect to both types of broadening, an increase in either the homogeneous or inhomogeneous line width results in broadening of the absorption spectrum without affecting the integrated intensity. However, an increase in the homogeneous line width results in both broadening and depression of the resonance Raman cross sections. Therefore, the absolute resonance Raman intensities of the symmetric stretch fundamental and overtone transitions can be used to partition

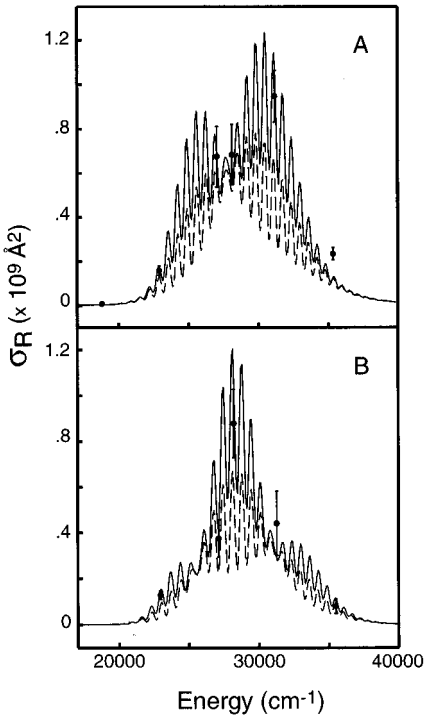

Figure 4. (A) Raman excitation profile for the symmetric stretch fundamental. The data are given by the points with corresponding values reported in Table 1. The dashed line is the calculation assuming that all broadening is homogeneous. The disagreement between the calculation and the data demonstrates that inhomogeneous broadening is also present. Best agreement with the data (solid line) is obtained with Gaussian homogeneous line width of 80 ± 15 cm^{-1} and inhomogeneous standard deviation of 160 ± 20 cm^{-1}. Other parameters used in the calculation are reported in Table 2. (B) Raman excitation profile for the symmetric stretch overtone. The data are given by the points with corresponding values reported in Table 1. Parameters for the calculation (solid line) are reported in Table 2.

between homogeneous and inhomogeneous broadening. Self-consistent modeling of the Raman and absorption cross sections resulted in a Gaussian line width of 80 ± 15 cm^{-1} and standard deviation of the Gaussian inhomogeneous distribution of 160 ± 20 cm^{-1}.

The use of absolute intensities to constrain the magnitude of the homogeneous line width is critical to the interpretation of the results presented below. Nonradiative decay of the $^2A_2$ surface is believed to occur via spin−orbit coupling to the $^2A_1$ surface. The increase in broadening evident in comparison of the absorption spectrum in cyclohexane relative to gas phase OClO (Figure 2) suggests that nonradiative decay of the optically prepared surface is more efficient in cyclohexane, potentially due to modulation of the $^2A_2$ and $^2A_1$ potential energy surface energies upon solvation. This expectation is consistent with the 80 cm^{-1} homogeneous line width corresponding to an optical dephasing time of 60 fs. Therefore, modulation of potential-energy surface interactions that can alter the $^2A_2$ excited-state decay rate are incorporated into this analysis through the homogeneous line width. Since absolute resonance Raman intensities constrain the homogeneous line width, they also constrain to what degree couplings between surfaces are modulated as reflected by population decay and/or vibronic dephasing. The increase in homogeneous line width in cyclohexane suggests that modulation of potential energy surface interactions may play a role in defining the chemistry of OClO. However, other effects including modulation of the $^2A_2$ potential energy surface topography may also be operative as will be discussed below.

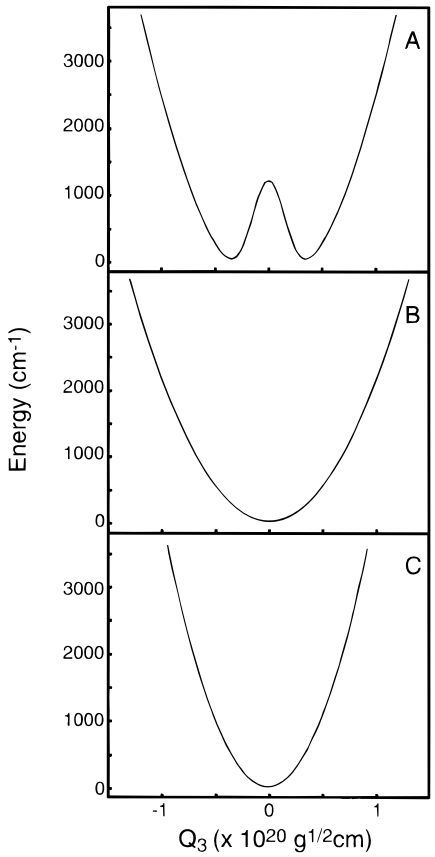

Figure 5. Potential energy surfaces employed for the asymmetric stretch coordinate of OClO. (A) Potential energy surface determined by analysis of the gas-phase absorption spectrum.[8] (B) Potential energy surface determind by ab initio theoretical analysis.[36] (C) Potential energy surface determined by the resonance Raman intensity analysis reported here. Parameters for each surface are reported in the text.

As an initial starting point in this analysis, the curvature and displacements of the $^2A_2$ state along the symmetric stretch, bend, and asymmetric stretch determined from analysis of the gas-phase absorption spectrum were employed as described above.[8] Even with adjustment of the displacements and anharmonicity along the symmetric stretch and bend, the gas-phase potential energy surface overestimates the observed asymmetric stretch overtone intensity. Figure 5A presents the experimentally determined gas-phase potential along the asymmetric stretch.[8] This potential is a harmonic well ($\omega = 571$ cm^{-1}) with a Gaussian barrier at the origin ($A = 1673$ cm^{-1} and $a^2 = 0.024$). In this previous absorption study, inclusion of the energy barrier was necessary to reproduce the overtone to second-overtone intensity ratio of the asymmetric stretch. This potential has been questioned by ab initio theoretical results which suggest that the potential along the asymmetric stretch coordinate is harmonic with $\omega_e = 437$ cm^{-1} (Figure 5B).[36] This surface was also employed in our analysis and also resulted in predicted intensity much larger than that observed (Figure 6). In these simulations, the symmetric stretch and bend parameters were adjusted to achieve best fit to the absorption spectrum and Raman cross sections with slight (<5%) differences in these parameters existing between fits. It was found that a harmonic description of the $^2A_2$ surface along the asymmetric stretch was able to reproduce the small overtone intensity given a reduction in excited-state frequency from 1100 to 750 ± 100 cm^{-1} (Figure 5C). In summary, the $^2A_2$ potential energy surface parameters determined by analysis of the gas-phase absorption spectrum or predicted from theory are apparently not accurate descriptions of the $^2A_2$ potential along the asymmetric stretch in cyclohexane.

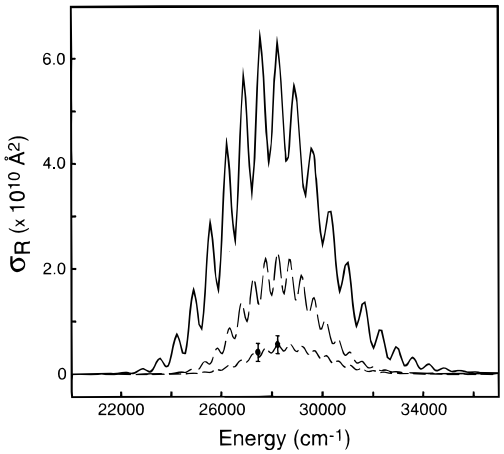

Figure 6. Resonance Raman excitation profile of the overtone of the asymmetric stretch. The data are given by the points and correspond to the values reported in Table 1. The predicted intensity for the overtone transition employing the gas-phase potential (solid), the ab initio potential (long dashed), and the harmonic potential determined from this analysis (short dashed) are presented. Both the gas-phase and ab initio potentials predict intensity roughly an order of magnitude larger than that observed. The observed overtone intensity in cyclohexane is consistent with a modest reduction in excited-state frequency from 1100 to 750 ± 100 cm^{-1}

Discussion

Asymmetric Stretch Overtone Intensity. The pattern of intensities observed in the resonance Raman spectra provides a detailed picture of the initial excited-state structural evolution of OClO. The most important result of this study involves the intensity of the asymmetric stretch. Figure 6 demonstrates that neither the experimentally determined nor the theoretically predicted $^2A_2$ surfaces along this coordinate are capable of reproducing the weak overtone intensity of this mode in solution. The origin of this result can be understood within the time-dependent framework of Raman scattering. Resonance Raman intensity corresponding to fundamental Stokes transitions ($\langle f| = \langle(i + 1)|$) is derived by propagation of the initial ground-state wave packet out of the Franck−Condon region, resulting in a buildup of overlap between this time-dependent state and the final state in the scattering process. By symmetry, the expectation value for the excited-state slope can be nonzero only for totally symmetric modes (the symmetric stretch and bend in the case of OClO in C_{2v} symmetry). Consistent with this, fundamental intensity corresponding to the asymmetric stretch is not observed on resonance.

Although the excited-state slope is zero for nontotally symmetric coordinates, change in the curvature of the excited-state potential energy surface relative to the ground state can result in overtone intensity. The potential energy surfaces used in this study to model the overtone intensity of the asymmetric stretch (Figure 5) are all of different curvature relative to the ground state; therefore, all are predicted to give rise to overtone intensity. However, the intensity derived from each of these surfaces is markedly different (Figure 6). Figure 7 presents the time-dependent overlap corresponding to the overtone transition of the asymmetric stretch for these surfaces. As this figure illustrates, the magnitude of the time-dependent overlap is largest for the double-well potential. The larger maximum amplitude of the time correlator demonstrates that the excursion of the wave packet away from the Franck−Condon region is greatest for this potential, and the short overlap buildup time results from rapid wave packet dynamics away from the Franck−Condon region caused by the large second-moment of the potential.

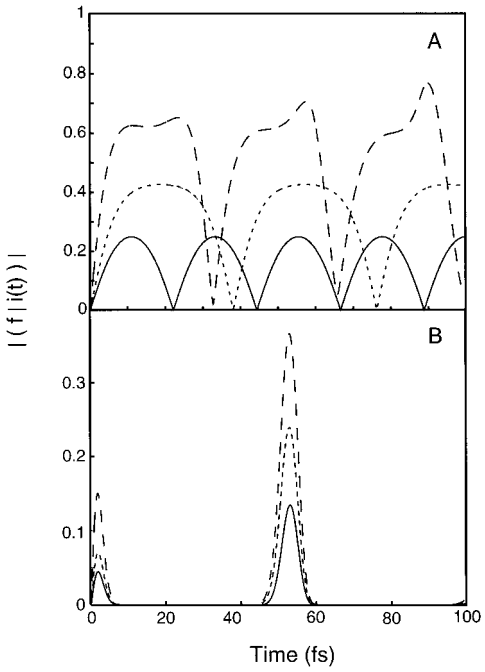

Figure 7. (A) Absolute value of the calculated time-dependent overlaps corresponding to the asymmetric stretch component of the asymmetric stretch overtone transition. Overlaps employing the gas-phase potential (long dashed), the ab initio potential (short dashed), and the potential determined from analysis of the Raman intensities (solid) are presented. (B) Product of the above overlaps with the $\langle 0|0(t)\rangle$ overlap along the symmetric stretch and the homogeneous line width. Larger overlap intensity results in a corresponding larger predicted Raman cross section such that the gas-phase potential (long dashed) results in the largest predicted intensity relative to the ab initio (short dashed) and proposed potentials (solid) as illustrated in Figure 6.

If a large homogeneous line width or displacement along multiple dimensions (the so-called "multimode effect") is operative, "short-time limit" scattering dynamics result such that only the early-time buildup of the time correlator is important in determining Raman intensity. In this limit, the relatively slow buildup of overlap generated by the asymmetric stretch potentials presented above would result in similar predictions of weak intensity in the overtone of the asymmetric stretch. The use of absolute resonance Raman intensities to constrain the homogeneous line width as described above combined with the limited nuclear dimensionality of OClO results in the later-time behavior of the Raman time correlator also contributing to the observed scattering such that the predicted intensity derived from the different models for the $^2A_2$ surface along the asymmetric stretch differ significantly. This effect is illustrated in Figure 7B where the time correlators derived from the three models of the asymmetric stretch potential depicted in Figure 7A are multiplied by $\langle 0|0(t)\rangle$ of the symmetric stretch and the homogeneous line width. The resulting overlaps demonstrate that both the initial dynamics and later-time behavior of the overall time correlator are important in defining the intensity for the overtone transition along the asymmetric stretch. Since an increase in time-correlator intensity results in an increase in scattering intensity, we expect the gas-phase potential to result in the largest predicted intensity as demonstrated in Figure 6.

The asymmetric stretch overtone intensity is consistent with a reduction in excited-state frequency relative to the ground state from 1100 to 750 ± 100 cm^{-1}. This small intensity is consistent with the lower amplitude and slower buildup time of the time correlator (Figure 7). Therefore, the barrier present in the gas phase along the asymmetric stretch coordinate either is not present or is dramatically reduced in solution. A comparable system in terms of nuclear dimensionality for which a resonance Raman intensity analysis has been performed is sulfur dioxide (SO_2).[72] In this system, the S_3 state is also bifurcated along the asymmetric stretch. The resonance Raman spectrum of SO_2 in hexane demonstrates no overtone intensity corresponding to the asymmetric stretch; however, this observation is not in disagreement with the predicted intensity employing the gas-phase potential. The apparent discrepancy between the applicability of gas-phase surfaces to predicted resonance Raman intensities of SO_2 and OClO in solution is consistent with the larger barrier along the asymmetric stretch in OClO.[27] Solvent perturbations of the barrier height in SO_2 may be subtle and difficult to ascertain; however, changes in the barrier along the asymmetric stretch in OClO are easier to determine given the large barrier height.

Dynamics on the $^2A_2$ Surface. Although the vibronic structure of the $^2B_1-{}^2A_2$ transition demonstrates that the $^2A_2$ state is predissociative, the initial structural evolution occurring on the optically prepared, excited-state surface provides the initial momentum along the reaction coordinate. Therefore, both the nature and time scale of evolution occurring on the $^2A_2$ state may be important in defining the photochemical fate of OClO. Analysis of the vibronic line widths observed in the gas-phase absorption spectrum suggests that the lifetime of the $^2A_2$ state is level dependent with values ranging from 20 to <1 ps.[9] In addition, transitions involving excitation of both the symmetric stretch and the bend or asymmetric stretch demonstrated a large increase in line width indicating that the bend and/or asymmetric stretch may serve to promote the decay of the optically prepared excited state.[9] In the analysis presented here, the homogeneous line width is incorporated such that consideration of level-dependent optical dephasing is not possible. Therefore, the line width reported here can be viewed as an average value. Given this, the Gaussian line width of 80 cm^{-1} corresponds an average optical dephasing time of ~60 fs. Partitioning of the homogeneous line width into pure dephasing and lifetime components can be performed if the fluorescence quantum yield is known. Current work in our laboratory involves the measurement of this quantity; however, the resonance Raman spectra reported here are presented without background subtraction demonstrating that the fluorescence from OClO is weak. This observation suggests that more rapid decay of the optically prepared excited state occurs in cyclohexane relative to the gas phase. One possible explanation for the apparent decrease in lifetime of the $^2A_2$ state is that stabilization of the various excited states of OClO due to solvation results in more efficient coupling of the $^2A_2$ state with the lower-lying, optically weak $^2B_2$ and $^2A_1$ states. Ab initio theoretical results predict that these two excited states are located within 0.2 eV of the Franck−Condon region of the $^2A_2$ surface. Solvation is expected to lower the energies of the three excited states to differing degrees due to the different geometries and electron densities in each state.[35,36] Evidence for state relaxation due to solvation is found in the ~2000 cm^{-1} reduction of the E_{00} energy of the $^2B_1$-$^2A_2$ transition in cyclohexane relative to the gas phase.[7,8,27] In addition, the deviation of the depolarization ratio of the symmetric stretch from 0.33 (Table 1) is consistent with other states participating in the scattering process. Although the $^2B_2$ state is predicted to be optically dark by symmetry, the $^2B_1-{}^2A_1$ transition is allowed and predicted to be orthogonal to the $^2B_1-{}^2A_2$ transition. Various experiments designed to ascertain the location of this state have been unsuccessful due to the apparent weak intensity of this transition.[4] The results presented here suggest that the increase in nonradiative decay of the $^2A_2$ excited state (potentially to the $^2A_1$ surface) may be one reason for the phase-

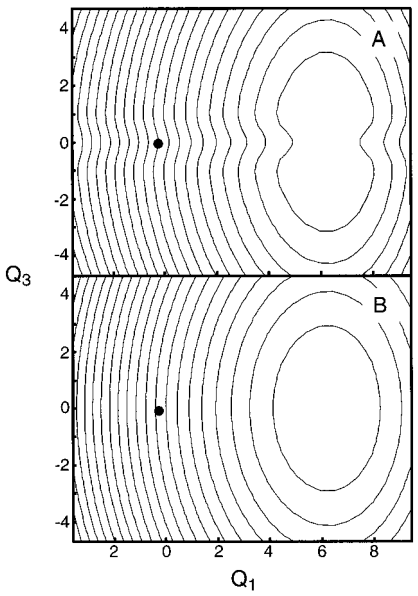

Figure 8. Two-dimensional contour plots of the $^2A_2$ potential energy surface along the symmetric (Q_1) and asymmetric (Q_3) stretch coordinates. (A) The gas-phase surface is constructed using the parameters reported by Richard and Vaida.[8] (B) The potential in cyclohexane determined from the resonance Raman intensity analysis presented here. Comparison of the plots demonstrates that in the gas phase, significant evolution along the asymmetric stretch occurs upon photoexcitation; however, little evolution along this coordinate occurs in solution.

dependent reactivity of OClO. To further investigate this possibility, the resonance Raman intensity analysis of OClO in a series of solvents of varying polarity and polarizability is underway in an attempt to correlate the reactivity of OClO with solvent-induced change in excited-state couplings and resulting decay of the optically prepared $^2A_2$ state.[56]

The analysis presented here illustrates that in addition to an increase in the decay rate of the $^2A_2$ surface, differences in excited-state structural evolution between the gas and condensed phase also exist. Figure 8 presents two-dimensional contour plots of the $^2A_2$ surface along the symmetric and asymmetric stretch both in the gas phase and in cyclohexane. The gas-phase potential is constructed from the analysis of the high-resolution gas-phase absorption spectrum performed by Richard and Vaida.[8] The excited-state displacements and frequencies of the bend are similar in both the gas and condensed phase, suggesting that evolution along this coordinate is not responsible for phase-dependent reactivity of OClO. Therefore, the bend is not included in Figure 8, and the discussion presented here focuses on the difference in evolution along the symmetric and asymmetric stretch coordinates. The figure illustrates that in the gas phase, relaxation out of the Franck−Condon region involves evolution along both coordinates. In particular, evolution along the symmetric stretch coordinate results in a bond length increase of 0.15 Å, and relaxation along the asymmetric stretch results in a bond-length change of ±0.06 Å. The sign of the displacement along the symmetric stretch (i.e., bond elongation) has been established by rotational spectroscopy[24,27,46,47] and is supported by ab initio theoretical work.[35,36] The experimentally determined double-well potential along the asymmetric stretch can be envisioned as resulting in ClO bond compression or elongation by 0.06 Å such that the combined evolution along both stretch coordinates results in an equilibrium excited-state structure in which ClO bond lengths are unequal. In contrast, although evolution along the symmetric stretch coordinate is comparable between the gas phase and cyclohexane, the barrier that exists in the gas phase along the asymmetric stretch is dramatically reduced or absent in solution. In cyclohexane, the combined evolution along the symmetric and asymmetric stretch coordinates results in an equilibrium excited-state geometry in which both ClO bonds are elongated, but of equal length. It is important to note that the conclusions stated here would be solidified by the presence of gas-phase resonance Raman data with current work in our laboratory designed to obtain this information.

Symmetry and OClO Photochemistry. The differences in excited-state structure described above suggest that initial, excited-state structural evolution may define the symmetry of the reaction coordinate. In the gas phase, evolution along the asymmetric stretch coordinate results in a lowering of molecular symmetry from C_{2v} in the $^2A_2$ excited state, but this symmetry is maintained in the excited state in cyclohexane. The symmetry under which the reaction proceeds defines the electronic state correlations and thus the reactivity of OClO.[4,7,12,35,49,73] Theory suggests that population of the $^2B_2$ state via decay of the $^2A_2$ surface is the mechanism for production of atomic chlorine and molecular oxygen with two possible pathways existing for photoproduct formation. Under C_{2v} symmetry, the $^2B_2$ state correlates directly with the $Cl(^2P_u) + O_2(^1\Delta_g)$ product channel where in C_s symmetry, the $^2B_2$ state correlates with the excited, A′ state of ClOO which can decay to form $Cl(^2P_u) + O_2(^1\Delta_g)$ or $O_2(^3\Sigma_g^-)$. However, excited-state internal conversion of ClOO to the ground-state A″ surface can precede dissociation in which case $Cl(^2P_u)$ and $O_2(^3\Sigma_g^-)$ are formed by ground-state decomposition of ClOO. Recent transient absorption studies of OClO in water provide support for the latter sequence of events.[11,12] Therefore, if C_{2v} symmetry is maintained during the course of the reaction, direct production of $Cl(^2P_u) + O_2(^1\Delta_g)$ is possible, but the lowering of symmetry should result in atomic chlorine production via ClOO. The important difference between these pathways is that the C_{2v} reaction coordinate results in the production of excited molecular oxygen where the C_s pathway combined with rapid ClOO internal conversion does not. The production of $O_2(^1\Delta_g)$ has been measured by monitoring emission corresponding to the $^1\Delta_g$ to $^3\Sigma_g^-$ transition.[49] In this study, an increase in the formation of electronically excited oxygen was observed with a reduction in solvent polarity, supporting the hypothesis that the decomposition of OClO in cyclohexane occurs via the higher symmetry reaction coordinate. Although structural evolution on the lower lying $^2A_1$ and $^2B_2$ excited states complicates this simple picture of events, the pattern of Raman intensities observed here suggests that the nuclear relaxation that occurs on the $^2A_2$ surface serves to define the symmetry under which the reaction proceeds.

Solvent−Solute Interactions. The nature of the solvent−solute interactions responsible for modification of the $^2A_2$ potential energy surface is the main question posed by the above results. The majority of research on solvent−solute interactions has focused on the mechanics of polar solvation.[74−76] A recent resonance Raman intensity analysis of I_3^- in polar solvents demonstrated that polar solvation dynamics directly influence the excited-state structural evolution of this compound due to charge localization which occurs in formation of the I_2^- and I photoproducts.[77] Studies on the vibrational relaxation of charged species in polar solvents have also demonstrated that dipole−dipole and charge−dipole interactions can dramatically affect the course of chemical reactions in solution.[78−84] However, nonpolar solvation dynamics must dominate the response of cyclohexane to OClO photoexcitation. The dynamics relevant to nonpolar solvation can be partitioned into two parts, a dielectric interaction involving dipole−induced dipole and induced dipole−induced dipole (i.e., van der Waals) coupling and mechanical forces representing the solvent response to the

change in solute geometry.[74,85−90] Recent transient hole-burning and time-resolved fluorescence studies have demonstrated that the mechanical response of the solvent can occur on the subpicosecond time scale[89,90] and thus will appear as homogeneous on the time scale of Raman scattering.[61,77] It is reasonable to assume that mechanical forces are involved in the response of cyclohexane to OClO excitation given the large geometry change of the solute upon photoexcitation. The restoring force provided by the solvent shell in response to this change in geometry would result in an increase in potential energy at large displacements along both coordinates, consistent with the observed effective increase in harmonic frequency along the asymmetric stretch. It should be noted that this interaction is expected to be significantly different for larger displacements such that the solvent−solute interaction at the minimum of the excited-state potential energy may be significantly different than in higher energy regions of this surface. In addition, the substantial decrease in the $^2B_1-^2A_2$ energy gap observed in cyclohexane relative to the gas phase stands in contrast to the modest Stokes shifts seen in other systems where mechanical interactions dominate.[85,89] This observation suggests that dipole−induced dipole interactions are also of importance.

The change in the molecular dipole moment is largest for displacement along the asymmetric stretch; therefore, evolution along this coordinate is expected to be strongly coupled to the solute dipole−solvent induced dipole interaction. The dipole moment of OClO in the ground, $^2B_1$ electronic state is 1.792 D, with the negative end of the dipole oriented toward the terminal oxygens.[36,91] Upon photoexcitation, theory predicts that the $^2A_2$, $^2A_1$, and $^2B_2$ states all have electron density shifted toward the terminal oxygens, with the extent of charge localization dependent on the specific structural relaxation which occurs on each surface.[35,36] The induced polarization of the solvent must respond to the dipole-moment change accompanying photoexcitation. In addition, excited-state evolution along the asymmetric stretch will result in the largest change in dipole moment relative to other coordinates such that the potential energy surface along the asymmetric stretch should be most sensitive to the solvent potential.[33,34,36] Determination of the effective solvent potential is not trivial with interactions between solvent molecules making a substantial contribution.[85,86] Therefore, the details of the solvent−solute interactions are difficult to predict. However, the polarizability of cyclohexane is relatively large (11 Å^3) suggesting that the magnitude of this interaction is substantial. For example, the thermally averaged interaction energy of a 1.79 D dipole and a spherical molecule with polarizability of 11 Å^3 at a separation of 3 Å is ∼25 cm^{-1}.[92] Further evidence for the importance of dipole−induced dipole forces in modifying the $^2A_2$ potential energy surface is found in previous resonance Raman studies of *cis*- and *trans*-hexatriene.[93−95] In this work, differences in the excited-state potential energy surface along the non-totally symmetric, central-double-bond torsion were observed between the gas and condensed phase with the frequency of the excited-state potential along this coordinate increasing from 110 to 199 cm^{-1} in solution. In addition, increase in the effective excited-state frequency of the torsion was correlated with an increase in solvent polarizability. This result suggests that the effect of solvent polarizability on potential enegy surfaces can be substantial; however, molecular dynamics simulations would be extremely helpful in defining the importance of dipole−induced dipole forces in modifying the $^2A_2$ potential. In addition, resonance Raman intensity analysis of OClO dissolved in solvents of varying polarity and polarizability will assist in determining the nature of solvent−solute interactions which define the structural relaxation occurring on the optically prepared excited state.[56]

Conclusion

In this paper, we have presented the resonance Raman intensity analysis of OClO dissolved in cyclohexane. Analysis of the absolute resonance Raman cross sections and electronic absorption spectrum demonstrates that upon excitation, structural evolution occurs along all three normal coordinates. However, the large structural change along the asymmetric stretch observed in the gas phase is not observed in solution. This change in structural evolution results in the ground-state C_{2v} symmetry being maintained in the excited state. This conservation of symmetry in the predissociative, $^2A_2$ state may result in this symmetry being preserved throughout the course of the reaction and thus affect the mechanism of photoproduct formation. In particular, the results presented here suggest that the excited-state reaction dynamics of OClO and mechanism of photoproduct formation will vary as a function of solvent polarity and/or polarizability. Current research in our laboratory is designed to ascertain the existence of and dynamical factors responsible for this behavior.

Acknowledgment is made to the donors of the Petroleum Research Fund, administered by the American Chemical Society, for support of this research. The National Science Foundation is also acknowledged for their support of this work through the CAREER program (CHE-9701717) P.J.R. is the recipient of a Camielle and Henry Dreyfus New Faculty Award. The Royalty Research Foundation of the University of Washington is also acknowledged for partial support of this work. We would like to thank the Chemistry Department at Seattle University for use of their absorption spectrometer. We would also like to thank Anne Myers and John Simon for their comments on this work and Veronica Vaida for providing the gas-phase absorption spectrum of OClO.

References and Notes

(1) Molina, M. J.; Molina, L. T.; Golden, D. M. *J. Phys. Chem.* **1996**, *100*, 12888.
(2) Vaida, V.; Frost, G. J.; Brown, L. A.; Naaman, R.; Hurwitz, Y. *Ber. Bunsen-Ges. Phys. Chem.* **1995**, *99*, 371.
(3) Rossky, P. J.; Simon, J. D. *Nature* **1994**, *370*, 263.
(4) Vaida, V.; Simon, J. D. *Science* **1995**, *268*, 1443.
(5) Graham, J. D.; Roberts, J. T.; Brown, L. A.; Vaida, V. *J. Phys. Chem.* **1996**, *100*, 3115.
(6) Brown, L. A.; Vaida, V.; Hanson, D. R.; Graham, J. D.; Roberts, J. T. *J. Phys. Chem.* **1996**, *100*, 3121.
(7) Vaida, V.; Goudjil, K.; Simon, J. D.; Flanders, B. N. *J. Mol. Liquids* **1994**, *61*, 133.
(8) Richard, E. C.; Vaida, V. *J. Chem. Phys.* **1991**, *94*, 153. Frost, G. J.; Goss, L. M.; Vaida, V. *J. Geophys. Res.-Atmos.* **1996**, *101*, 3879.
(9) Richard, E. C.; Vaida, V. *J. Chem. Phys.* **1991**, *94*, 163.
(10) Vaida, V.; Solomon, S.; Richard, E. C.; Ruhl, E.; Jefferson, A. *Nature* **1989**, *342*, 405.
(11) Chang, Y. J.; Simon, J. D. *J. Phys. Chem.* **1996**, *100*, 6406.
(12) Dunn, R. C.; Flanders, B. N.; Simon, J. D. *J. Phys. Chem.* **1995**, *99*, 7360.
(13) Dunn, R. C.; Simon, J. D. *J. Am. Chem. Soc.* **1992**, *114*, 4856.
(14) Dunn, R. C.; Richard, E. C.; Vaida, V.; Simon, J. D. *J. Phys. Chem.* **1991**, *95*, 6060.
(15) Bishenden, E.; Donaldson, D. J. *J. Chem. Phys.* **1994**, *101*, 9565.
(16) Bishenden, E.; Donaldson, D. J. *J. Chem. Phys.* **1993**, *99*, 3129.
(17) Bishenden, E.; Haddock, J.; Donaldson, D. J. *J. Phys. Chem.* **1991**, *95*, 2113.
(18) Delmdahl, R. F.; Baumgärtel, S.; Gericke, K.-H. *J. Chem. Phys.* **1996**, *104*, 2883.
(19) Baumert, T.; Herek, J. L.; Zewail, A. H. *J. Chem. Phys.* **1993**, *99*, 4430.
(20) Davis, H. F.; Lee, Y. T. *J. Phys. Chem.* **1992**, *96*, 5681.

(21) Lawrence, W. G.; Clemitshaw, K. C.; Apkarian, V. A. *J. Geophys. Res.* **1990**, *95*, 18591.
(22) Flesch, R.; Wassermann, B.; Rothmund, B.; Rühl, E. *J. Phys. Chem.* **1994**, *98*, 6263.
(23) Rühl, E.; Jefferson, A.; Vaida, V. *J. Phys. Chem.* **1990**, *94*, 2990.
(24) Hamada, Y.; Merer, A. J.; Michielsen, S.; Rice, S. A. *J. Mol. Spectrosc.* **1981**, *86*, 499.
(25) Michielsen, S.; Meyer, A. J.; Rice, S. A.; Novak, F. A.; Freed, K. F.; Hamada, Y. *J. Chem. Phys.* **1981**, *74*, 3089.
(26) McDonald, P. A.; Innes, K. K. *Chem. Phys. Lett.* **1978**, *59*, 562.
(27) Brand, J. C. D.; Redding, R. W.; Richardson, A. W. *J. Mol. Spectrosc.* **1970**, *34*, 399.
(28) Mueller, H. S. P.; Willner, H. *J. Phys. Chem.* **1993**, *97*, 10589.
(29) Johnsson, K.; Engdahl, A.; Ouis, P.; Nelander, B. *J. Mol. Struct.* **1993**, *293*, 137.
(30) Lanzendorf, E. J.; Kummel, A. C. *Geophys. Res. Lett.* **1996**, *23*, 1521.
(31) Pursell, C. J.; Conyers, J.; Alapat, P.; Parveen, R. *J. Phys. Chem.* **1995**, *99*, 10433.
(32) Adrian, F. J.; Bohandy, J.; Kim, B. F. *J. Chem. Phys.* **1986**, *85*, 2692.
(33) Arkell, A.; Schwager, I. *J. Am. Chem. Soc.* **1967**, *89*, 5999.
(34) Rochkind, M. M.; Pimentel, G. C. *J. Chem. Phys.* **1967**, *46*, 4481.
(35) Gole, J. L. *J. Phys. Chem.* **1980**, *84*, 1333.
(36) Peterson, K. A.; Werner, H.-J. *J. Chem. Phys.* **1992**, *96*, 8948.
(37) Burkholder, J. B.; Talukdar, R. K.; Ravishankara, A. R. *Geophys. Res. Lett.* **1994**, *21*, 585.
(38) Rowland, F. S. *Annu. Rev. Phys. Chem.* **1991**, *42*, 731.
(39) Solomon, S.; Sanders, R. W.; Miller Jr., H. L. *J. Geophys. Res.* **1990**, *95*, 13807.
(40) Hoigné, J.; Bader, H. *Water Res.* **1994**, *28*, 45.
(41) Tratnyek, P. G.; Hoigné, J. *Water Res.* **1994**, *28*, 57.
(42) Huang, C. P.; Dong, C.; Zhonghung, T. *Waste Management* **1993**, *13*, 361.
(43) Owens, J. W. *Environ. Tox. Chem.* **1991**, *10*, 1511.
(44) Kolar, J. J.; Lindgren, B. O.; Pettersson, B. *Wood Sci. Technol.* **1983**, *17*, 117.
(45) Ortigoso, J.; Escribano, R.; Burkholder, J. B.; Lafferty, W. J. *J. Mol. Spectrosc.* **1992**, *155*, 25.
(46) Krishna Pillai, M. G.; Curl, R. F. *J. Chem. Phys.* **1962**, *37*, 2921.
(47) Coon, J. B. *J. Chem. Phys.* **1946**, *14*, 665.
(48) Johnsson, K.; Engdahl, A.; Ouis, P.; Nelander, B. *J. Phys. Chem.* **1992**, *96*, 5778.
(49) Dunn, R. C.; Anderson, J. L.; Foote, C. S.; Simon, J. D. *J. Am. Chem. Soc.* **1993**, *115*, 5, 5307.
(50) Brauer, G. *Handbook of Preparative Inorganic Chemistry*; Academic Press: New York, 1963; Vol. 1.
(51) Masschelein, W. J. *Chlorine Dioxide. Chemistry and Environmental Impact of Oxychlorine Compounds*; Ann Arbor Science Publishers, Inc.: Ann Arbor, MI, 1979.
(52) Mortensen, O. S.; Hassing, S. In *Advances in Infrared and Raman Spectroscopy*; Clark, R. J. H., Ed.; Heyden: London, 1980; Vol. 6; p 1.
(53) Trulson, M. O.; Mathies, R. A. *J. Chem. Phys.* **1986**, *84*, 2068.
(54) Lawless, M. K.; Mathies, R. A. *J. Chem. Phys.* **1992**, *96*, 8037.
(55) Fodor, S. P. A.; Rava, R. P.; Hays, T. R.; Spiro, T. G. *J. Am. Chem. Soc.* **1985**, *107*, 1520.
(56) Foster, C.; Esposito, A.; Reid, P. J., manuscript in preparation.
(57) Lee, S.-Y.; Heller, E. J. *J. Chem. Phys.* **1979**, *71*, 4777.
(58) Tannor, D. J.; Heller, E. J. *J. Chem. Phys.* **1982**, *77*, 202.
(59) Heller, E. J.; Sundberg, R. L.; Tannor, D. *J. Phys. Chem.* **1982**, *86*, 1822.
(60) Myers, A. B.; Mathies, R. A. In *Biological Applications of Raman Spectrometry*; Spiro, T. G., Ed.; John Wiley & Sons, Inc.: New York, 1987; Vol. 2; pp 1−58.
(61) Myers, A. B. *J. Opt. Soc. Am. B* **1990**, *7*, 1665.
(62) Fraga, E.; Webb, M. A.; Loppnow, G. R. *J. Phys. Chem.* **1996**, *100*, 3278.
(63) Sue, J.; Mukamel, S. *J. Chem. Phys.* **1988**, *88*, 651.
(64) Sue, J.; Yan, Y. J.; Mukamel, S. *J. Chem. Phys.* **1986**, *85*, 462.
(65) Feit, M. D.; Fleck, J. A. *J. Chem. Phys.* **1983**, *78*, 301.
(66) Feit, M. D.; Fleck, J. A.; Steiger, A. *J. Comput. Physics* **1982**, *47*, 412.
(67) Dunn, R. C.; Flanders, B. N.; Vaida, V.; Simon, J. D. *Spectrochim. Acta* **1992**, *48A*, 1293.
(68) Hubinger, S.; Nee, J. B. *Chem. Phys.* **1994**, *181*, 247.
(69) Davies, J. A.; Mason, N. J.; Marston, G.; Wayne, R. P. *J. Phys. B: At. Mol. Opt. Phys.* **1995**, *28*, 4179.
(70) Eysel, H. H.; Bernstein, H. J. *J. Raman. Spectrosc.* **1977**, *6*, 140−145. Bourgeois, M. T.; Jacon, M.; Van Labecke, D.; Eysel, H. H. *J. Raman. Spectrosc.* **1977**, *6*, 146.
(71) Lawless, M. K.; Reid, P. J.; Mathies, R. A. In *Ultrafast Dynamics of Chemical Systems*; Simon, J. D., Ed.; Kluwer: Amsterdam, 1994; p 267.
(72) Yang, T.-S.; Myers, A. B. *J. Chem. Phys.* **1991**, *95*, 6207.
(73) Shuler, K. E. *J. Chem. Phys.* **1953**, *21*, 624.
(74) Stratt, R. M.; Maroncelli, M. *J. Phys. Chem.* **1996**, *100*, 12981.
(75) Maroncelli, M. *J. Mol. Liquids* **1993**, *57*, 1.
(76) Barbara, P. F.; Jarzeba, W. *Adv. Photochem.* **1990**, *15*, 1.
(77) Johnson, A. E.; Myers, A. B. *J. Chem. Phys.* **1995**, *102*, 3519.
(78) Benjamin, I.; Barbara, P. F.; Gertner, B. J.; Hynes, J. T. *J. Phys. Chem.* **1995**, *99*, 9, 7557.
(79) Walhout, P. K.; Alfano, J. C.; Thakur, K. A. M.; Barbara, P. F. *J. Phys. Chem.* **1995**, *99*, 7568.
(80) Banin, U.; Rhuman, S. *J. Chem. Phys.* **1993**, *98*, 4391.
(81) Harris, A. L.; Brown, J. K.; Harris, C. B. *Annu. Rev. Phys. Chem.* **1988**, *39*, 341.
(82) Benjamin, I.; Banin, U.; Rhuman, S. *J. Chem. Phys.* **1993**, *98*, 8337.
(83) Whitnell, R. M.; Wilson, K. R.; Hynes, J. T. *J. Chem. Phys.* **1992**, *96*, 5354.
(84) Heilweil, E. J.; Doany, F. E.; Moore, R.; Hochstrasser, R. M. *J. Chem. Phys.* **1982**, *76*, 5632.
(85) Stratt, R. M.; Adams, J. E. *J. Chem. Phys.* **1993**, *99*, 775.
(86) Dobrosavljevic, V.; Henebry, C. W.; Stratt, R. M. *J. Chem. Phys.* **1988**, *88*, 5781.
(87) Roy, S.; Bagchi, B. *J. Chem. Phys.* **1994**, *100*, 8802.
(88) Ma, J.; Vanden Bout, D.; Berg, M. *J. Chem. Phys.* **1995**, *103*, 9146.
(89) Berg, M. *Chem. Phys. Lett.* **1994**, *228*, 317.
(90) Fourkas, J. T.; Benigno, A.; Berg, M. *J. Chem. Phys.* **1993**, *99*, 8552.
(91) Tanaka, K.; Tanaka, T. *J. Mol. Spectrosc.* **1983**, *98*, 425.
(92) *CRC Handbook of Chemistry and Physics*, 74th ed.; CRC Press: Boca Raton, FL, 1993. Winn, J. S. *Physical Chemistry*; Harper Collins College Publishers: New York, 1995.
(93) Ci, X.; Pereira, M. A.; Myers, A. B. *J. Chem. Phys.* **1990**, *92*, 4708.
(94) Ci, X.; Myers, A. B. *J. Chem. Phys.* **1992**, *96*, 6433.
(95) Myers, A. B.; Phillips, D. L.; Ci, X.; Westerfield, C.; Rodier, J.-M. *Proc. SPIE*; Nafie, L. A., Mantsch, H. H., Eds.; 1993; Vol. 1890, pp 83−94.
(96) Li, B.; Myers, A. B. *J. Phys. Chem.* **1990**, *94*, 4051.
(97) Karplus, M.; Porter, R. N. *Atoms and Molecules*; W. A. Benjamin, Inc.: New York, 1970.